VNU Journal of Science: Earth and Environmental Sciences, Vol. 39, No. 3 (2023) 54-62

VNU Journal of Science: Earth and Environmental Sciences

Journal homepage: https://js.vnu.edu.vn/EES

Original Article

Using a Novel Heterojunction $CoWO_4$/g-C_3N_4 as Visible Light Photocatalyst for Photodegradation of Organic Pollutant

Do Van Dang*, Tran Thi Chi Linh, Le Thanh Son

VNU University of Science, 19 Le Thanh Tong, Hoan Kiem, Hanoi, Vietnam

Received 22 May 2023
Revised 22 June 2023; Accepted 14 August 2023

Abstract: Methylene Blue (MB) is a common dye that has various applications in different fields, including medicine, biology, and environmental science. While it can be beneficial in certain contexts, it can also have negative effects on the environment under certain circumstances. In this study, the photodegradation of MB under visible light irradiation using a novel heterojunction $CoWO_4$/g-C_3N_4 catalyst was investigated. A series of $CoWO_4$/g-C_3N_4 composites were synthesized and characterized using various techniques, including XRD, SEM, SEM-EDS, FT-IR, and UV-DRS. The results revealed that the 0.3$CoWO_4$/g-C_3N_4 composite showed the highest efficiency (93%) in degrading MB during the 80-minute photodegradation process, aligning with the pseudo-first-order kinetics. The results provide clear evidence that the formation of $CoWO_4$/g-C_3N_4 heterojunction greatly enhances the efficiency of photocatalysis by facilitating the swift separation of electron-hole pairs and boosting the redox capability. Additionally, the photodegradation efficiency remained above 90% even after four cycles, suggesting the stability of the catalyst.

Keywords: Methylene Blue, $CoWO_4$, g-C_3N_4, visible light.

1. Introduction

The textile industry, a major sector globally, is responsible for approximately 20% of the pollution in industrial water. This industry heavily relies on synthetic materials, leading to excessive use of chemicals, water, and energy [1]. As a result, the wastewater released from textile processes contains harmful dye molecules, posing a significant threat to the environment. Methylene blue (MB), a widely used cationic dye in textile production, is particularly problematic due to its toxicity and widespread application [2]. To address this environmental risk, it is necessary to treat the

* Corresponding author.
E-mail address: dangdovan@hus.edu.vn

https://doi.org/10.25073/2588-1094/vnuees.4953

wastewater from textile production before it is discharged into the environment. MB present in textile wastewater is known to be resistant to biodegradation and photodegradation [3]. Traditional methods like oxidation [4], microbial treatment [5], ozonation [6], absorption [7], and nanofiltration [8] have not been successful in effectively removing dyes from wastewater. On the other hand, photocatalysis has emerged as a promising technique for efficient removal of MB and various dyes, offering advantages such as fast mineralization, simple design and operation, and cost-effectiveness [9].

Importantly, when light energy is equal to or greater than the energy gap of a photocatalyst that illuminates it, a photochemical reaction takes place on the surface of the catalyst. This reaction results in the formation of electron-hole pairs, which then degrades harmful organic pollutants into smaller molecules like H_2O and CO_2 [9]. Numerous photocatalytic materials, including common semiconductors, plasmonic nanoparticles, and 2D nanomaterials, have been extensively studied [9]. Among those, g-C_3N_4, a metal-free photocatalyst, has garnered significant attention in academic circles. It has gained popularity due to its semiconductor nature. This material exhibits intriguing characteristics, including remarkable chemical stability, a distinctive electron configuration, a rapid charge transfer rate, and the use of low-cost precursors such as urea, thiourea, and melamine. Furthermore, g-C_3N_4 is known for its low toxicity and possesses a suitable band structure of around 2.7 eV, enabling it to absorb roughly 7% of solar energy during photocatalytic processes. Despite its interesting properties, the charge carrier dynamics of g-C_3N_4, including charge separation and transfer, can be relatively inefficient. This can lead to the recombination of photogenerated electron-hole pairs, reducing the overall photocatalytic efficiency [10].

To overcome these problems, various attempt has been made to reduce the recombination of electron-hole pairs and enhance the overall efficiency of g-C_3N_4 including co-catalyst incorporation [11], hybridization with other materials [12], elemental doping [13], or its self-modification [14]. There has been an increasing focus on metal tungstate (MWO_4) materials in recent years due to their distinct chemical and optical characteristics. Among them, $CoWO_4$ has gained significant attention in photocatalysis because of its narrow band gap and its ability to be easily excited by visible light [15,16]. The valence band (VB) and conduction band (CB) potentials of $CoWO_4$ are approximately 3.15 and 0.35 V, respectively. These properties make it compatible with g-C_3N_4 and enable the formation of a Z-scheme heterojunction [17-20]. This heterojunction enhances their light absorption capacity and extends the lifetime of the generated charge carriers. In 2019, Prabavathi et al., reported the construction of heterostructure $CoWO_4$/g-C_3N_4 nanocomposite as an efficient visible-light photocatalyst for norfloxacin degradation [17]. It was observed that the degradation rate of norfloxacin using a combination of $CoWO_4$ and g-C_3N_4 photocatalysts was 3.18 times faster compared to pure g-C_3N_4, and 2.69 times faster compared to pure $CoWO_4$. This enhanced photocatalytic activity can be attributed to the synergistic effect between $CoWO_4$ nanoparticles and g-C_3N_4 nanosheets, which effectively suppresses the rapid recombination of photogenerated electron-hole (e^- - h^+) pairs. Two years later, the $CoWO_4$@g-C_3N_4 nano-composites were fabricated by a reflux-calcination method for enhancing removal of ciprofloxacin [18]. Very recently, the photodegradation of tetracycline hydrochloride, Ciprofloxacin, and Norfloxacin using heterojunction $CoWO_4$/g-C_3N_4 as visible light photocatalyst was also investigated by Yue et al., [20].

Following these investigations, in this study, we put our effort into the construction of a $CoWO_4$/g-C_3N_4 heterojunction for the efficient photocatalytic degradation of MB under visible light irradiation.

2. Experimental

2.1. Chemicals

Melamine ($C_3H_6N_6$, 99%), cobalt nitrate hexahydrate ($Co(NO_3)_2.6H_2O$, 99%), sodium tungstate dihydrate ($Na_2WO_4.2H_2O$, 99.5%), Methylene Blue ($C_{16}H_{18}ClN_3S$, 95%) were purchased from China. All compounds were used directly without further purification.

2.2. Catalyst Preparation

$CoWO_4$ nanoparticles were prepared following our previous report [17, 18]. Firstly, 4 mmol of $Co(NO_3)_2.6H_2O$ was added to 50 mL of distilled water, followed by the dropwise addition of a 0.08 M Na_2WO_4 solution. The suspension was stirred for 4 hours, and the resulting precipitate was separated via centrifugation and dried at 60 °C for 24 hours before being transferred to a furnace. The furnace was heated continuously to 500 °C with a rate of 5 °C per minute and kept at that temperature for 2 hours to obtain $CoWO_4$.

g-C_3N_4 was prepared following the previous report published anywhere [10]. Melamine was calcinated at 550 °C for 4 h to prepare g-C_3N_4 as a yellow powder.

To synthesize the $CoWO_4$/g-C_3N_4 heterojunction, a mixture of $CoWO_4$ and g-C_3N_4 with varying mass ratios of $CoWO_4$ was sonicated in 100 mL of distilled water for 1 hour. The resulting suspension was heated in an autoclave at 160 °C for 12 hours. The solid was filtered and washed with water to obtain the x$CoWO_4$/g-C_3N_4 composite (x = 0.2, 0.3, and 0.4, respectively).

2.3. Characterizations

Standard powder X-ray diffraction (XRD) patterns were collected using a D8-Advance-Brucker instrument. Fourier transform infrared spectroscopy (FTIR) spectra were acquired using a Bruker TENSOR-27 spectrometer. Scanning electron micrograph (SEM) images of the synthesized materials were captured using a Hitachi S-4800 microscope. Scanning Electron Microscopy with Energy Dispersive Spectroscopy (SEM-EDS) images were obtained using an Oxford instrument equipped with the X-stream 2 detector (EDX pulse processor). Optical properties were analyzed by recording ultraviolet-visible light absorption spectra (UV-Vis) using a Hitachi UH4150 spectrophotometer.

2.4. Photodegradation of MB

In a typical procedure, 50 mg of catalysts were mixed with 100 mL of a 10 mg/L MB solution and stirred in the absence of light for 30 minutes until adsorption-desorption equilibrium was achieved. Afterward, the mixture was exposed to a 200 W LED in a photoreactor positioned 5 cm away from the deflection reflector. Samples of 2 mL were withdrawn every 20 minutes during the irradiation period and filtrated by 0.2 microfilters before measurement using a UV-VIS spectrophotometer (F7G32AA/Agilent) at a wavelength of 665 nm.

For comparison purposes, the direct photolysis of MB without a catalyst (using only light) was also investigated under the same conditions. The percentage (%) of MB removal was determined using Equation (1), while Equation (2) was utilized to calculate the kinetics of MB dye removal through the photocatalytic process based on the first-order reaction kinetics and corresponding time. In the equations, C_0 represents the initial concentration of the MB solution at adsorption-desorption equilibrium ($mg.L^{-1}$), C_t represents the final concentration of the dye solution after treatment ($mg.L^{-1}$), and k (min^{-1}) represents the reaction kinetic rate constant for a first-order process.

$$\% \text{ Removal} = \frac{C_o - C_t}{C_o} \times 100 \quad (1)$$

$$\ln \frac{C_o}{C_t} = k.t \quad (2)$$

To assess the reusability of the photocatalyst, it was recovered after the reaction by centrifugation, washed with ethanol and distilled water, and then dried under vacuum at 60 °C for 6 hours before being employed for the next cycle.

3. Results and Discussion

3.1. Characterizations of Synthesized Materials

Figure 1 displayed the XRD patterns of pure $CoWO_4$, g-C_3N_4, and $CoWO_4$/g-C_3N_4 composite with varying amounts of $CoWO_4$ (20%, 30%, and 40%). The XRD pattern of pure $CoWO_4$ shows the diffraction peaks at 2θ of 19.2°, 23.9°, 24.8°, 30.8°, 38.8°, 41.6°, 54.3°, and 65.4°, which can be indexed as the (001), (110), (0110, (111), (200), (002), (121), (202), and (113) planes, respectively. The result indicated that the patterns disclosed the standard for typical monoclinic crystal wolframite planes of $CoWO_4$ according to JCPDS: 15-0867 [18, 19]. In addition, the absence of information on other Cobalt, or tungstate products from the XRD pattern further confirmed the successful preparation of $CoWO_4$. The g-C_3N_4 material exhibited a broad peak at 2θ values of 27.8° in its X-ray diffraction (XRD) pattern. The peak at 27.8° corresponded to the (002) crystal plane of the conjugated aromatic system (JCPDS: 50-1512) [14].

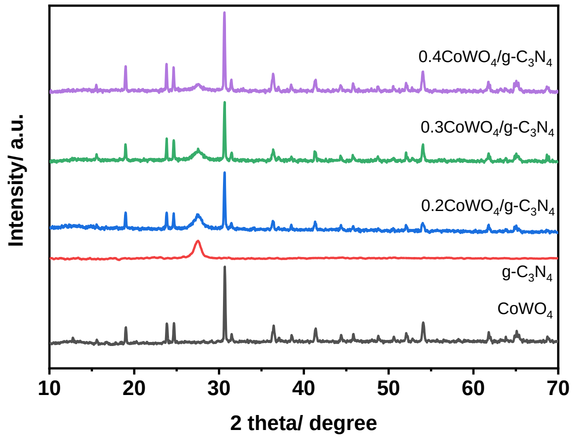

Figure 1. XRD patterns of $CoWO_4$, g-C_3N_4, and $CoWO_4$/C_3N_4 composite.

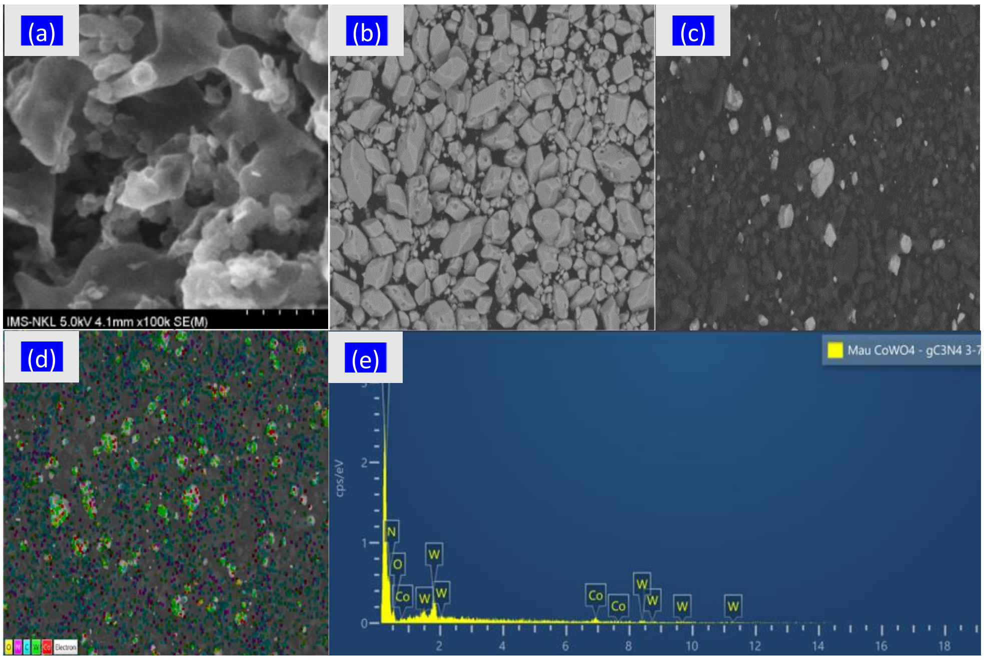

Figure 2. SEM images of (a) g-C_3N_4, (b) $CoWO_4$, (c) 0.3$CoWO_4$/g-C_3N_4 composite, (d) SEM-EDS of 0.3$CoWO_4$/g-C_3N_4 composite, (e) SEM-EDX of 0.3$CoWO_4$/g-C_3N_4.

It is important to note that the XRD patterns of $CoWO_4$ and g-C_3N_4 were still discernible in the $CoWO_4$/g-C_3N_4 composite without the decrease in intensity. These findings suggest that the composite maintained its structured regularity during construction, which is consistent with earlier studies.

The morphology of pure $CoWO_4$, g-C_3N_4, and 0.3$CoWO_4$/g-C_3N_4 composite was examined through SEM images (Figure 2). The SEM images showed that the polymerization of g-C_3N_4 resulted in the excellent distribution of nanolayer structures (Figure 2a). It was apparent that the synthesized $CoWO_4$ sample was made up of nanocubes that were assembled randomly (Figure 2b). However, due to the presence of g-C_3N_4 in the cluster of $CoWO_4$, it was difficult to detect $CoWO_4$ nanoparticles in the $CoWO_4$/g-C_3N_4 composite (Figure 2c). SEM-EDS analysis of the 0.3$CoWO_4$/g-C_3N_4 composite's elemental composition and distribution is shown in Figure 2d. The findings revealed that $CoWO_4$ was uniformly dispersed in g-C_3N_4, with no other atoms detected, indicating successful composite synthesis. Furthermore, the SEM-EDX results allowed the fitting of the element's components to the composite's formula (Figure 2e).

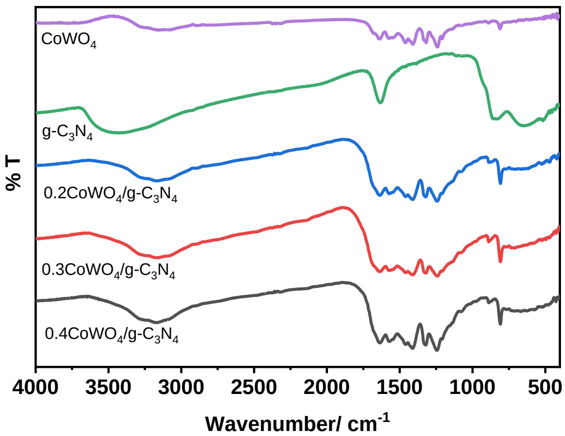

Figure 3. FT-IR of $CoWO_4$, g-C_3N_4, and $CoWO_4$/g-C_3N_4 composite.

Figure 3 illustrates the FT-IR spectra of g-C_3N_4, $CoWO_4$, and x$CoWO_4$/g-C_3N_4 composite, which were examined to further confirm the success of the composite. The FT-IR spectrum of g-C_3N_4 has 2 peaks at 810 and 3200 cm^{-1}, which corresponded to the tris-triazine units' breathing modes and residual N–H groups, respectively. Furthermore, peaks ranging from 1200 cm^{-1} to 1700 cm^{-1} were caused by the stretching vibration modes of the C-N group and the C=N group's stretching. The strong broadband detected in the 400-1000 cm^{-1} low-frequency region in Figure 3b was attributed to the characteristic deformation modes of Co-O, W-O, and W-O-W bridges of $CoWO_4$. The appearance of bands at 820 cm^{-1} was related to the O-W-O vibration mode. The $CoWO_4$/g-C_3N_4 FT-IR spectrum had similar peaks to those of g-C_3N_4 and $CoWO_4$ with lower peak intensities because of the deposition of $CoWO_4$ on the g-C_3N_4.

It was well known that the optical properties of a catalyst are crucial in determining its photoactivity. To investigate the effect of $CoWO_4$ nanoparticles incorporation on g-C_3N_4, the UV-DRS spectra of pure g-C_3N_4 and $CoWO_4$/g-C_3N_4 composite with varying $CoWO_4$ content were analyzed (refer to Figure 4). Pure g-C_3N_4 exhibited a strong absorption region near 400 nm, while the presence of $CoWO_4$ on the surface of g-C_3N_4 caused a redshift towards longer wavelengths compared to g-C_3N_4 and increased absorption in the visible light range.

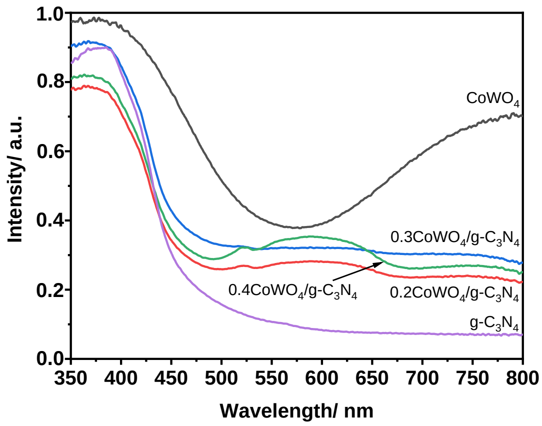

Figure 4. UV-DRS of $CoWO_4$, g-C_3N_4, and $CoWO_4$/g-C_3N_4 composite.

The bandgap of all materials was determined through Tauc plots based on matching DRS absorption spectra. The Tauc plots of g-C_3N_4 and $CoWO_4$/g-C_3N_4 are presented in Figure 5. The bandgap of x$CoWO_4$/g-C_3N_4 (with 20, 30, and 40 wt% of $CoWO_4$) produced values of 2.45 eV, 2.37 eV, and 2.43 eV, respectively, which were considerably lower than that of pure g-C_3N_4 (2.60 eV). These findings indicate that $CoWO_4$/g-C_3N_4 materials are more active than g-C_3N_4 when exposed to visible light.

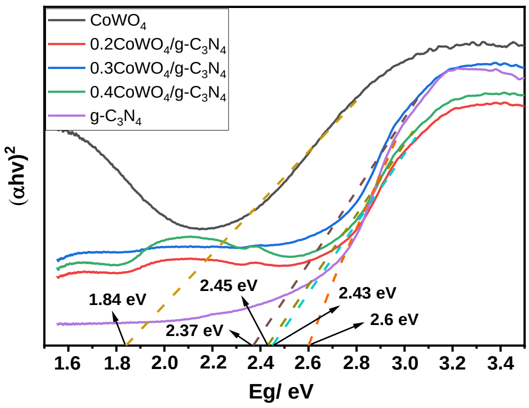

Figure 5. Tauc plot of $CoWO_4$, g-C_3N_4, and $CoWO_4$/g-C_3N_4 composite.

3.2. Photodegradation of MB

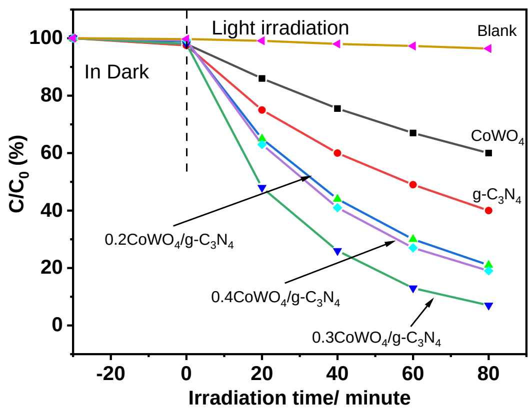

Figure 6. Photodegradation of MB using $CoWO_4$, g-C_3N_4, $CoWO_4$/g-C_3N_4, and without catalysts.

The photocatalytic ability of the $CoWO_4$/g-C_3N_4 composite was investigated in the degradation of MB in water under visible light (Figure 6).

There was no significant degradation of MB, indicating a minimal decrease due to surface adsorption in the absence of light. However, under visible light, the degradation of MB was moderate yield despite the low bandgap (1.84 eV) of the $CoWO_4$ photocatalyst, while the value of C_3N_4 was 60%, as the photogenerated electron and hole pairs recombined quickly. Increasing the loading amount of $CoWO_4$ on g-C_3N_4 from 20% to 30% resulted in a substantial increase of approximately 79% and 93% in MB removal, respectively. This enhancement was attributed to the decrease in the bandgap from 2.45 to 2.37 eV, making the composite more active under visible light. The inhibition of electron-hole recombination, supported by UV-DRS and PL spectra, further confirmed the improved photocatalytic activity. Interestingly, the presence of 0.4$CoWO_4$/g-C_3N_4 catalyst led to a slight decrease in MB degradation yield (81%), coincident with its higher bandgap of 2.43 eV. This can be explained by the significant amount of $CoWO_4$ hindering the light absorption of g-C_3N_4, which is responsible for dye breakdown, thus resulting in reduced photocatalytic activity. Moreover, the photodegradation of MB was almost negligible in the absence of a catalyst under visible light. Based on these findings, the 0.3%$CoWO_4$/g-C_3N_4 composite was selected as the photocatalyst for subsequent experiments.

To investigate the reaction kinetics of MB degradation by $CoWO_4$/g-C_3N_4, the photodegradation data was analyzed using a pseudo-first-order model (Eqn. 2). The relationship between $\ln(C_0/C)$ and the exposure time for MB degradation on the catalysts is depicted in Figure 7. The photodegradation curve exhibited a close adherence to the pseudo-first-order kinetics for all cases. The model was employed to calculate the rate constants (k) for each catalyst, which were then plotted in Figure 7. As the $CoWO_4$ loading on the surface of g-C_3N_4 increased, the rate constants also showed an increase. Among the photocatalysts, the 0.3$CoWO_4$/g-C_3N_4 catalyst demonstrated the highest rate constant (0.03292 min^{-1}) for MB degradation, surpassing the values reported in recent studies for other photocatalysts.

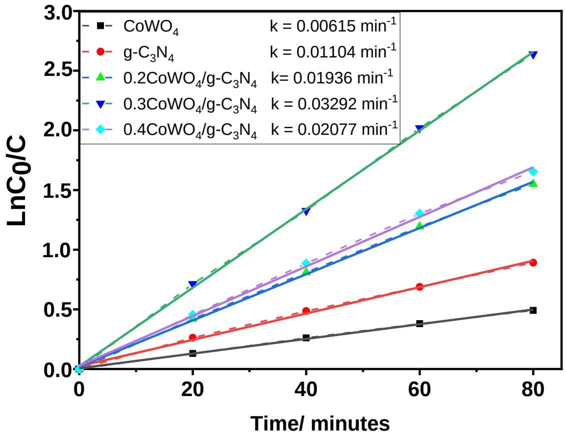

Figure 7. Pseudo-first-order model of photodegradation of MB using synthesized catalysts.

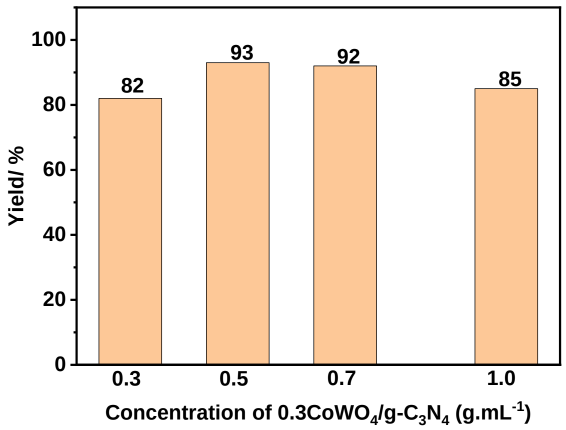

Figure 8. Effect of catalyst concentration for removal of MB.

A series of experiments were undertaken to investigate the influence of varying amounts of $0.3CoWO_4/g\text{-}C_3N_4$ catalyst on the elimination of MB. The catalyst quantities ranged from 0.3 to 1.0 $g.L^{-1}$ while maintaining a constant concentration of 10 $mg.L^{-1}$ MB and a pH of 7.0. The findings, depicted in Figure 8, revealed a noteworthy enhancement in the removal of MB when the catalyst amount increased from 0.3 to 0.5 $g.L^{-1}$. It could be explained by the increase of active sites in accordance with the increase of $CoWO_4$ amount. Nevertheless, higher concentrations of the catalyst did not yield further improvements in the photodegradation of MB. This outcome may be attributed to the catalyst's suspension, which hindered the penetration of light to the MB molecules.

Finally, the recycle ability of $0.3CoWO_4/g\text{-}C_3N_4$ for the photodegradation of MB was investigated, and the findings are presented in Figure 9. After an 80-minute irradiation period, the photocatalytic degradation efficiencies were determined to be 92%, 91.5%, and 90% for the second, third, and four cycles, respectively. These results suggest that $0.3CoWO_4/g\text{-}C_3N_4$ demonstrates high stability and can be employed for long-term degradation processes.

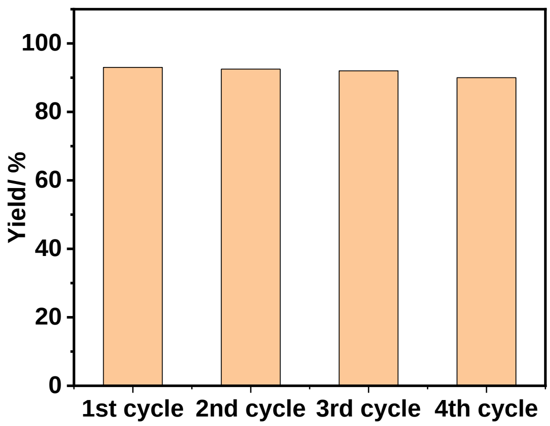

Figure 9. Recycle ability of $0.3CoWO_4/g\text{-}C_3N_4$ for photodegradation of MB.

4. Conclusion

The research reported the $CoWO_4/g\text{-}C_3N_4$ nanocomposite for efficient degradation of MB under visible light irradiation. The findings obtained from XRD, FT-IR, and SEM analyses confirm the preservation of the $g\text{-}C_3N_4$ structure even after incorporating $CoWO_4$, as supported by the SEM-EDS analysis. The UV-DRS results indicate that the $CoWO_4/g\text{-}C_3N_4$ materials exhibit higher activity compared to $g\text{-}C_3N_4$. Notably, the $0.3CoWO_4/g\text{-}C_3N_4$ composite demonstrates a significant enhancement in the photodegradation of MB within 80 minutes of visible light irradiation. Moreover, the $0.3CoWO_4/g\text{-}C_3N_4$ photocatalyst proves to be stable and can be reused at least three times without any decline in its photocatalytic effectiveness, making it highly suitable for practical applications.

Acknowledgements

This work has been supported by Vietnam National University (Project QG.23.13).

References

[1] A. A. Inyinbor, F. A. Adekola, G. A. Olatunji, Kinetics, Isotherms and Thermodynamic Modeling of Liquid Phase Adsorption of Rhodamine B Dye onto Raphia Hookerie Fruit Epicarp, Water Resour Ind, Vol. 15, 2016, pp. 14-27, https://doi.org/10.1016/J.WRI.2016.06.001.

[2] J. Cheng, C. Zhan, J. Wu, Z. Cui, J. Si, Q. Wang, X. Peng, L. S. Turng, Highly Efficient Removal of Methylene Blue Dye from an Aqueous Solution Using Cellulose Acetate Nanofibrous Membranes Modified by Polydopamine, ACS Omega, Vol. 5, 2020, pp. 5389-5400, https://doi.org/10.1021/ACSOMEGA.9B04425.

[3] R. S. P. Mak, E. L. Liebelt, Methylene Blue: An Antidote for Methemoglobinemia and Beyond, Pediatr Emerg Care., Vol. 37, 2021, pp. 474-477, https://doi.org/10.1097/PEC.0000000000002526.

[4] L. Li, Y. Zhao, J. J. Wang, H. Chen, H. Li, J. Wang, Y. Wang, Y. Bai, D. Dang, the $[CuI_4Cl_4]$ Cluster of A Coordination Complex Based on Polypyridyl Ligand for Heterogeneous Fenton-Like MB Degradation Without Illumination and Electrocatalytic Reduction of H_2O_2 and $K_2Cr_2O_7$, Dyes and Pigments, Vol. 207, 2022, pp. 110763, https://doi.org/10.1016/J.DYEPIG.2022.110763.

[5] W. Wang, J. Jiang, C. Zhang, Q. Zhao, K. Wang, J. Lv, Micro-Electricity Utilization Performance and Microbial Mechanism in Microbial Fuel Cell Powered Electro-Fenton System for Azo Dye Treatment, Biochem. Eng. J, Vol. 186, 2022, pp. 108583, https://doi.org/10.1016/J.BEJ.2022.108583.

[6] X. Liu, Y. Hou, J. Guo, Y. Wang, Q. Zuo, C. Wang, Catalytic Ozone Aqueous Decomposition of Methylene Blue Using Composite Metal Oxides, IOP Conf Ser Mater Sci Eng, Vol. 87, 2015, pp. 012031, https://doi.org/10.1088/1757-899X/87/1/012031.

[7] G. Zhou, Q. Wang, R. Song, S. Li, S. Yang, Q. Zhang, Synthesis of Core-Double-Shell Structured Fe_3O_4@PDA/HKUST-1: Characterization Analysis and Adsorption Performance on Cationic MB Dyes, Journal of Physics and Chemistry of Solids, Vol. 172, 2023, pp. 111094, https://doi.org/10.1016/J.JPCS.2022.111094.

[8] L. Yang, F. Jia, Z. Juan, D. Yu, L. Sun, Y. Song, Y. Wang, L. Huang, J. Tang, High-Permeable Graphene Oxide/Graphitic Carbon Nitride Composite Nanofiltration Membrane For Selective Separation of Dye and Desalination, J Environ Chem Eng, Vol. 11, 2023, pp. 109306, https://doi.org/10.1016/J.JECE.2023.109306.

[9] V. H. Huong, T. C. Nguyen, C. D. Sai, N. H. Pham, A. B. Ngac, T. B. Nguyen, H. V. Bui, V. P. Vu, B. T. Nguyen, L. V. Dang, T. T. H. Le, T. T. Nguyen, D. V. Do, Facile Synthesis of ZnO/Ag Nanostructure with Enhanced Photocatalytic Activity, Chemnanomat, Vol. 9, No. 6, 2023, pp. e202300080, https://doi.org/10.1002/CNMA.202300080.

[10] H. T. T. Duong, M. T. P. Duong, O. K. Nguyen, S. T. Le, L. V. Dang, B. T. Nguyen, D. V. Do, Photocatalytic Activity of Ti-SBA-15/C_3N_4 for Degradation of 2,4-Dichlorophenoxyacetic Acid in Water under Visible Light, J. Anal. Methods Chem, 2022, ID 5531219, https://doi.org/10.1155/2022/5531219.

[11] Q. Zhong, H. Lan, M. Zhang, H. Zhu, M. Bu, Preparation of Heterostructure $g\text{-}C_3N_4$/ZnO Nanorods for High Photocatalytic Activity on Different Pollutants (MB, RhB, Cr(VI) and Eosin), Ceram Int, Vol. 46, 2020, pp. 12192-12199, https://doi.org/10.1016/J.CERAMINT.2020.01.265.

[12] Y. Zhang, J. Zhou, Q. Feng, X. Chen, Z. Hu, Visible Light Photocatalytic Degradation of MB Using Uio-66/$g\text{-}C_3N_4$ Heterojunction Nanocatalyst, Chemosphere, Vol. 212, 2018, pp. 523-532, https://doi.org/10.1016/J.Chemosphere.2018.08.117.

[13] S. Li, M. Zhang, P. Li, L. Ma, K. Peng, J. Zhao, Y. Liu, R. Wang, Boosting Visible-Light-Driven Photocatalytic Performance by Heterostructure of S-Doped $g\text{-}C_3N_4$/MIL-101(Fe), Inorg Chem Commun, Vol. 151, 2023, pp. 110616, https://doi.org/10.1016/J.INOCHE.2023.110616.

[14] X. Lian, Y. Li, Y. Zou, D. An, Q. Wang, Q. Zhou, X. Li, High Vis-Light Photocatalytic Property of $g\text{-}C_3N_4$ on Four Pollutants (RhB, MB, TC-HCl and p-Nitrophenol), Current Applied Physics, Vol. 39,

2022, pp. 196-204, https://doi.org/10.1016/J.CAP.2022.04.020.

[15] K. Leeladevi, M. Arunpandian, J. V. Kumar, T. Chellapandi, G. Mathumitha, J. W. Lee, E. R. Nagarajan, $CoWO_4$ Decorated Zno Nanocomposite: Efficient Visible-Light-Activated Photocatalyst for Mitigation of Noxious Pollutants, Physica B Condens Matter, Vol. 626, 2022, pp. 413493, https://doi.org/10.1016/j.physb.2021.413493.

[16] J. Wei, Z. Liu, Y. Zhang, Z. Yang, Z. Sun, Y. Li, Z. Cheng, Unraveling Charge Transfer Pathways and Mechanisms in Cds@$CoWO_4$ Z-Scheme Heterojunction Photocatalysts for High-Efficiency Environmental Remediation, Sep Purif Technol, Vol. 306, 2023, pp. 122664, https://doi.org/10.1016/j.seppur.2022.122664.

[17] S. L. Prabavathi, K. Govindan, K. Saravanakumar, A. Jang, V. Muthuraj, Construction of Heterostructure $CoWO_4$/g-C_3N_4 Nanocomposite as An Efficient Visible-Light Photocatalyst for Norfloxacin Degradation, Journal of Industrial And Engineering Chemistry, Vol. 80, 2019, pp. 558-567, https://doi.org/10.1016/j.jiec.2019.08.035.

[18] S. Sahoo, A. Behera, S. Mansingh, B. Tripathy, K. Parida, Facile Construction of $CoWO_4$ Modified g-C_3N_4 Nanocomposites with Enhanced Photocatalytic Activity under Visible Light Irradiation, Mater Today Proc, Vol. 35, 2021, pp. 193-197, https://doi.org/10.1016/j.matpr.2020.04.246.

[19] H. Ashiq, N. Nadeem, A. Mansha, J. Iqbal, M. Yaseen, M. Zahid, I. Shahid, g-C_3N_4/Ag@$CoWO_4$: A Novel Sunlight Active Ternary Nanocomposite for Potential Photocatalytic Degradation of Rhodamine B Dye, Journal of Physics and Chemistry of Solids, Vol. 161, 2022, pp. 110437, https://doi.org/10.1016/j.jpcs.2021.110437.

[20] C. Yue, J. Jiang, M. Li, X. Wang, T. Li, Z. Zhao, S. Dong, Accelerating the Peroxymonosulfate Activation and Charge Transfer by Construction of Fermi Energy Level-Matched $CoWO_4$/g-C_3N_4 Photocatalyst for Typical Antibiotics Degradation, Sep Purif Technol, Vol. 301, 2022, pp. 122020, https://doi.org/10.1016/j.seppur.2022.122020.